Implications for Lithospheric Reheating Beneath the African Superswell from P_{nl} Wave Propagation in Central and Southern Africa

Andrew A. Nyblade[1], Kristin S. Vogfjord[2], and Charles A. Langston[1]

[1]Department of Geosciences
Penn State University
University Park, PA 16802

[2]Department of Geological and Geophysical Sciences
Princeton Univeristy
Princeton, NJ

ABSTRACT

The African superswell is an extensive topographic anomaly comprising the eastern and southern African plateaus, and an area of elevated bathymetry in the southeastern Atlantic Ocean basin. By comparing the P-wave velocity structure of unrifted Proterozoic lithosphere beneath (e.g., southern Africa) and away from (e.g., central Africa) the African superswell, we investigate the hypothesis that uplift within the superswell distal to the Cenozoic East African rift valleys has been caused by lithospheric reheating. If lithospheric reheating is the primary cause of uplift within the superswell, then P-wave velocity gradients beneath the southern Africa should be about 0.001 s^{-1} lower than beneath central Africa. Lithospheric P-wave velocity structure is obtained by forward modeling of P_{nl} waveforms from four moderate sized earthquakes. Results suggest that upper mantle beneath central and southern Africa is similar, characterized by a lid structure with a constant velocity. There appears to be little evidence for (1) mantle velocity gradients beneath southern Africa that are lower than beneath central Africa, (2) a low velocity zone as shallow as 120 km beneath central Africa, and (3) the existence of a pronounced, shallow ($\leq$ 80 km depth) low velocity zone beneath southern Africa. Additionally, modeling results yield an average thickness of 45 km for Proterozoic crust beneath central Africa and 40 km beneath southern Africa, and somewhat slower crustal velocities beneath central Africa compared to southern Africa. The similarity in upper mantle structure between central and southern Africa suggests that uplift away from the Cenozoic East African rifts is not caused entirely by reheating of the lithosphere, but the possibility that a small amount of lithospheric reheating may have occurred cannot be ruled out. If, as our results suggest, uplift away from the East African rifts is not due primarily to lithospheric reheating, then additional explanations for the origin of the African superswell must be sought, either in conjunction with a small amount of lithospheric reheating or in isolation.

OBJECTIVE

The African superswell is one of the largest (areally) topographic anomalies on Earth, comprising three contiguous regions, each characterized by about 500 m of positive residual elevation; the eastern African plateau, the southern African plateau, and an area of the southeastern Atlantic Ocean basin southwest of the African continent (Nyblade and Robinson, 1994). The eastern and southern African plateaus have mean elevations of ~1 km, roughly 500 m higher than the mean global elevation of continents not covered by ice caps, while bathymetry in the southeastern Atlantic Ocean basin is about 500 m shallower than predicted by boundary layer cooling models (e.g., half-space and plate models) describing the age-dependence of bathymetry (Nyblade and Robinson, 1994). The northern boundary of the superswell on the African continent is shown in Figure 1.

Recent seismic work in Kenya, East Africa, clearly reveals that rifted lithosphere within the African superswell has been perturbed thermally (e.g., Green et al., 1991; KRISP working group, 1991; Braile et al., 1994; Slack et al., 1994; Keller et al., 1994), and therefore much of the superswell topography proximal to the Cenozoic East African rifts can be attributed to isostatic uplift from lithospheric reheating and also possibly to a component of dynamic support. However, the origin of elevated topography in unrifted areas of the African superswell is less certain. One possibility is that lithospheric reheating has also caused isostatic uplift away from the Cenozoic rifts, and in this paper we investigate that possibility. Reheating of the lithosphere as a possible explanation for superswell topography away from the Cenozoic rifts was previously suggested by Nyblade and Robinson (1994) based on the observation that heat flow from Proterozoic terrains in southern Africa, as well as from seafloor older than ~80 Ma in the oceanic portion of the African superswell, is slightly elevated. Similarly, interpretations of long-wavelength   (> 1000 km) Bouguer gravity anomalies in eastern and southern Africa also suggest that unrifted superswell lithosphere may be thermally altered (e.g., Wohlenberg, 1975; Fairhead, 1976; Fairhead and Revees, 1977; Brown and Girdler, 1980; Ebinger et al., 1989).

To investigate the lithospheric reheating hypothesis for the origin of the African superswell, we first model the P-wave velocity structure of Proterozoic lithosphere inside (southern Africa) and outside (central Africa) the African superswell, and then compare velocity models to identify structural differences caused by reheating. If the superswell lithosphere has been reheated, then the P-wave velocity structure of uppermost mantle beneath the African superswell should be different from that of "normal" (i.e., thermally unperturbed) upper mantle outside the superswell. Importantly, in this approach we focus on terrains of similar age (Proterozoic) beneath and away from the African superswell so that we can minimize the possibility of confusing structure resulting from lithospheric reheating with structure resulting from age-dependent thermal and compositional variations, such as those typically found between thinner, warmer Proterozoic lithosphere and thicker, colder Archean lithosphere (Jordan, 1988; Nyblade and Pollack, 1993a).

RESEARCH RESULTS

The P-wave velocity models that we use in this study are derived by forward modeling of P_{nl} waveforms from four earthquakes. The P_{nl} phase is a long-period waveform recorded at regional distances (< ~15°). It begins with the initial P arrival, continues through to the S wave arrival, and consists of two parts, upper mantle phases (Pn), and partially trapped crustal phases (PL). Hence the name P_{nl} (Helmberger and Engen, 1980; Wallace, 1983; Shaw and Orcutt, 1984). More specifically, the P_n portion of the waveform comprises P wave interactions with the uppermost mantle, for example, the headwave along the Moho and turning waves within the lid, while PL is a long-period wavetrain following P_n that propagates as partially trapped P-SV reverberations in the

crust, leaking SV wave energy into the mantle. In comparison to P_n wave propagation, PL wave propagation is relatively insensitive to mantle structure (Shaw and Orcutt, 1984).

The source-receiver paths used in this study can be seen in Figure 1 and details of the earthquakes are given in Table 1. Event 1 is located on the eastern flank of the Lake Tanganyika Rift and was recorded 1626 km to the northwest at Bangui (BCAO) in the Central African Republic. The ray path for Event 1 crosses the northern margin of the Congo Basin, lying outside the African superswell. Event 2 occurred in the tip of South Africa and was recorded at Windhoek (WIN), Namibia, 1193 km to the north. Events 3 and 4 occurred in Zambia and were recorded, respectively, 1183 and 1203 km to the southwest at Windhoek. The ray paths for these events cross Proterozoic mobile belts within the African superswell. Focal mechanisms show normal faulting with primarily E-W extension for Events 1, 3, and 4, and sinistral strike-slip motion for Event 2.

Green's functions were calculated using the wave number integration algorithm of Barker (1984) for point sources in elastic plane-layered structure. Anelastic attenuation was included by assuming complex layer velocities, with complex phase to produce a causal attenuation operator (Baag and Langston, 1986). Helmberger's (1973) earth flattening transformation was applied to velocity models prior to inclusion in the Green's functions calculations.

We begin by modeling lithospheric structure away from the African superswell to establish a reference model for thermally unperturbed lithosphere and then examine structure beneath the superswell. Two criteria are used to evaluate the "goodness" of fit between the observed and synthetic waveforms, (1) the P_n/PL amplitude ratio, and (2) the overall similarity between the observed and synthetic waveforms. The P_n/PL amplitude ratio, which we take as the ratio of the largest amplitude (peak to trough) within the P_n phase to the largest amplitude within the PL phase, is particularly sensitive to mantle velocity gradients because any P wave energy turning within the upper mantle, as a result of a positive velocity gradient, will boost the P_n amplitude relative to the PL amplitude.

Starting model parameters have been taken from two seismic refraction surveys across the Namaqua and Damara Belts (Figure 1) (Green and Durrheim, 1990; Baier et al., 1983). Velocities and layer thicknesses from these surveys have been averaged to produce a model with three crustal layers, a crustal thickness of 40 km, and an uppermost mantle velocity of 8.05 km s^{-1} (Table 2). For crustal attenuation, we assigned values of 1000 and 440 to Qp and Qs, respectively, and for the mantle we used values of 500 and 220 for Qp and Qs, respectively. Although the mantle Qp and Qs values are higher than average continental values, they are not unreasonable for Precambrian shield areas (e.g., Brune and Dorman, 1963).

The vertical and radial seismograms for Event 1 together with the synthetics from several models are shown in Figure 2. Distinct P_n and PL phases are seen on both components of motion. Figure 3 gives details of the velocity models, where Model 1 is the starting model described in Table 2. The synthetic waveforms for Model 1 show good resemblance to the data, with the P_n/PL amplitude ratio on both components of motion only slightly underestimating the observed ratios. However, the PL phase arrives ~10 seconds early relative to P_n (Figure 2), suggesting that the model can be improved.

The PL-P_n time can be increased in a number of ways. For example, crustal velocities can be lowered, making PL arrive later in the wavetrain, the crust can be thickened, also making PL arrive later, or the upper mantle velocity can be increased, making P_n arrive earlier. Combinations of these possibilities would also increase the PL-P_n time. To test these and other possibilities, synthetics for models with various crustal thicknesses and velocities were generated, and the three models which best match the data are shown in Figure 3a (Models 2, 3 and 4). Our preferred crustal model (Model 4,

Figure 3a) has a 45 km thick crust and velocities that are slightly lower than those in our starting model.

In Model 4, the P_n/PL amplitude ratio is only slightly overestimated on the vertical component of motion and only slightly underestimated on the radial component of motion, suggesting that a constant velocity lid may be a reasonable characterization of uppermost mantle structure beneath central Africa. But can alternative upper mantle models produce a better match in the P_n/PL amplitude ratios? Based on structure modeling in other Precambrian shield areas (e.g., King and Calcagnile, 1979; LeFevre and Helmberger, 1989), there are two likely possibilities; (1) the upper mantle might have a positive velocity gradient, and (2) the upper mantle could comprise a lid with a positive velocity gradient overlying a low velocity zone (LVZ).

Three alternative upper mantle models are shown in Figure 3b (Models 5, 6 and 7). To examine the effects of an upper mantle velocity gradient, a small velocity gradient of 0.001 s^{-1} was incorporated in Model 5. In this model the bottoming depth of P-waves is ~140 km. To examine the effects of a LVZ, Models 6 and 7 contain mantle lids with positive velocity gradients of 0.001 s^{-1} and 0.003 s^{-1}, respectively, overlying 30 km thick low velocity zones that begin at a depth representative of the base of the lithosphere, 120 km. In Model 6 rays bottom just below the LVZ, while in Model 7 rays bottom somewhat deeper. In all three models (5, 6 and 7) the P_n/PL amplitude ratio is significantly overestimated for both components of motion (Figure 2), and we therefore conclude that there is little evidence for (1) a mantle lid beneath central Africa containing a positive velocity gradient or (2) a low velocity zone as shallow as 120 km depth. Thus, our preferred model for the upper mantle beneath central Africa is a half-space (Model 4, Figure 6a). The existence of a low velocity zone deeper than 120 km, however, cannot be ruled out, given the depths at which the P-waves bottom in our models.

The data and synthetics for the source-receiver paths inside the African superswell (Events 2, 3 and 4) are shown in Figures 4, 5 and 6, and the accompanying velocity models are illustrated in Figure 7. Similar to Event 1, clear P_n and PL phases can be seen for Events 2, 3 and 4. Model 1 comprises the starting crustal model (Table 2), and examination of Figures 4, 5 and 6 reveals that for this model there is good resemblance between the synthetics and the data; the synthetic PL-P_n times are similar to the observed times, and the observed and calculated P_n/PL amplitude ratios are in reasonable agreement. The starting model is sufficient for explaining the major features of the data. Alternative models were tested and are shown; these models have various undesirable characteristics.

CONCLUSIONS AND RECOMMENDATIONS

Forward modeling of P_{nl} waveforms from four earthquakes within the southern African subcontinent suggest that Proterozoic upper mantle beneath central and southern Africa is similar, characterized by a constant velocity. Modeling results do not support the presence of a low velocity zone as shallow as 120 km beneath central Africa or the existence of a pronounced, shallow ($\leq$ 80 km depth) low velocity zone beneath southern Africa. The presence of deeper low velocity zones beneath central and southern Africa cannot be ruled out. These results are broadly consistent with the velocity models published by Clouser and Langston (1990), as well as the results of global tomography studies showing fast regions within the upper mantle beneath southern and central Africa (Su et al., 1994; Woodward and Masters, 1991). Additionally, our modeling results suggest an average thickness of 45 km for Proterozoic crust beneath central Africa and 40 km beneath southern Africa, and somewhat slower crustal velocities beneath central Africa compared to southern Africa.

The lack of evidence in our modeling analysis for mantle velocity gradients beneath Proterozoic terrains in southern Africa that are lower than beneath Proterozoic

terrains in central Africa suggests that the African superswell away from the Cenozoic East African rifts is not caused solely by reheating of the lithosphere. Furthermore, the lack of evidence in our modeling analysis for a pronounced low velocity zone beneath southern Africa, when combined with global seismic tomography models, suggests, albeit weakly, that significant thermal erosion of the base of the superswell lithosphere has also not occurred.

References

Baag, C-E., and C.A. Langston, Diffracted Sp generated under the Australian Shield, *J. Geophys. Res., 91*, 9507-9516, 1986.

Baier, B., H. Berckhemer, D. Gajewski, R.W. Green, C. Grimsel, and C. Prodehl, Deep seismic soundings in the area of the Damara Orogen, Nambia, South West Africa, in Intercontinental Fold Belts, edited by by H, Martin and F. Eder, Springer-Verlag, Berlin, pp. 885-900, 1983.

Barker, J.S., A seismological analysis of the May 1980 Mammoth Lakes, California earthquakes, Ph.D. thesis, Penn State Univ., University Park, 1984.

Braile, L.W., B. Wang, C.R. Daudt, G.R. Keller, and J.P. Patel, Modeling the 2-D seismic velocity structure across the Kenya rift, *Tectonophysics, 236*, 251-269, 1994.

Brown, C., and R.W. Girdler, Interpretation of African gravity and its implication for the breakup of the continents, *J. Geophys. Res., 85*, 6443-6455, 1980.

Brune, J., and J. Dorman, Seismic waves and Earth structure in the Canadian Shield, *Bull. Seis. Soc. Am., 53*, 167-209, 1963.

Clouser, R.H., and C.A. Langston, Upper mantle structure of southern Africa from P_{nl} waves, *J. Geophys. Res., 95*, 17403-17415, 1990.

Ebinger, C.J., T.D. Bechtel, D.W. Forsyth, and C.O. Bowin, Effective elastic plate thickness beneath the East African and Afar plateaus and dynamic compensation of the uplifts, *J. Geophys. Res., 94*, 2883-2901, 1989.

Fairhead, J.D., The structure of the lithosphere beneath the eastern rift, East Africa, deduced from gravity studies, *Tectonophys., 30*, 269-298, 1976.

Fairhead, J.D., and C.V. Reeves, Teleseismic delay times, Bouguer anomalies and inferred thickness of the African lithosphere, *Earth Planet. Sci. Lett., 36*, 63-76, 1977.

Green, R.W.E., and R.J. Durrhiem, A seismic refraction investigation of the Namaqualand Metamorphic Complex, South Africa, *J. Geophys. Res., 95*, 19927-19932, 1990.

Green, W.V., U. Achauer, and R.P. Meyer, A three-dimensional seismic image of the crust and upper mantle beneath the Kenya rift, *Nature, 354*, 199-203, 1991.

Helmberger, D.V., and G.R. Engen, Modeling the long-period body waves from shallow earthquakes at regional ranges, *Bull. Seis. Soc. Am., 70*, 1699-1714, 1980.

Helmberger, D.V., Numerical seismograms of long-period body waves from seventeen to forty degrees, *Bull. Seis. Soc. Am., 62*, 325-341, 1973.

Jordan, T.H., Structure and formation of the continental tectosphere, *J. Petrol., Spec. Lithosphere Issue*, 11-37, 1988.

Keller, G.R., C. Prodehl, J. Mechie, K. Fucks, M.A. Khan, P.K.H. Maguire, W.D. Mooney, U. Achauer, P.M. Davis, R.P. Meyer, L.W. Braile, I.O. Nyambok, and G.A. Thompson, The East African rift system in the light of KRISP 90, *Tectonophysics, 236*, 465-483, 1994.

King, D.W., and G. Calcagnile, P wave velocities in the upper mantle beneath Fennoscandia and western Russia, *Geophys. J. R. Astron. Soc., 46*, 407-432, 1976.

Krisp Working Party, Large-scale variation in lithospheric structure structure along and across the Kenya Rift, *Nature, 354*, 223-227, 1991.

Langston, C.A., Barker, J.S., and G.B. Pavlin, Point-source inversion techniques, *Phys. Earth Planet. Inter., 30*, 228-241, 1982.

LeFever, L.V., and D.V. Helmberger, Upper mantle P velocity structure of the Canadian shield, *J. Geophys. Res., 94*, 17749-17765, 1989.

Nyblade, A.A., and S.W. Robinson, The African Superswell, *Geophys. Res. Lett., 21*, 765-768, 1994.

Nyblade, A.A., and H.N. Pollack, A global analysis of heat flow from Precambrian terrains: Implications for the thermal structure of Archean and Proterozoic lithosphere, *J. Geophys. Res., 98*, 12207-12218, 1993a.

Shaw, P., and J. Orcutt, Propagation of PL and implications for the structure of Tibet, *J. Geophys. Res., 89*, 3135-3152, 1984.

Slack, P.D., P.M. Davis, KRISP Teleseismic working group, Attenuation and velocity of P-waves in the mantle beneath the East African Rift, Kenya, *Tectonophysics, 236,* 331-358, 1994.

Su, W. R.L. Woodward, and A.M. Dziewonski, Degree 12 model of shear velocity heterogeneity in the mantle, *J. Geophys. Res., 99,* 6945-6980, 1994.

Wallace, T.C., Long period regional body waves, Ph.D. thesis, Calif. Inst. of Technol., Pasadena, 1983.

Wohlenberg, J., The structure of the lithosphere beneath the East African Rift zones from interpretation of Bouguer anomalies, in *Afar Depression of Ethiopia,* 2, edited by A. Pilger and A. Rosler, Schweizerbart, Stuttgart, pp. 125-130, 1975.

Woodward, R.L., and G. Masters, Global upper mantle structure from long-period differential travel times, *J. Geophys. Res., 96,* 6351-6377, 1991.

Table 1. Earthquake Parameters.

Event	Date	Strike	Dip	Rake	m_b	M_0 (10^{24} dyne-cm)	Depth (km)
1	6/29/86	191.4	81.1	-72.0	5.0	2.9	36
2	9/29/69	123.5	89.4	-0.58	5.6	37.6	4
3	5/15/68	49.1	39.8	263.2	5.7	3.32	28
4	12/2/68	20.3	40.2	264.8	5.9	4.38	6

Table 2. Starting Velocity Model.

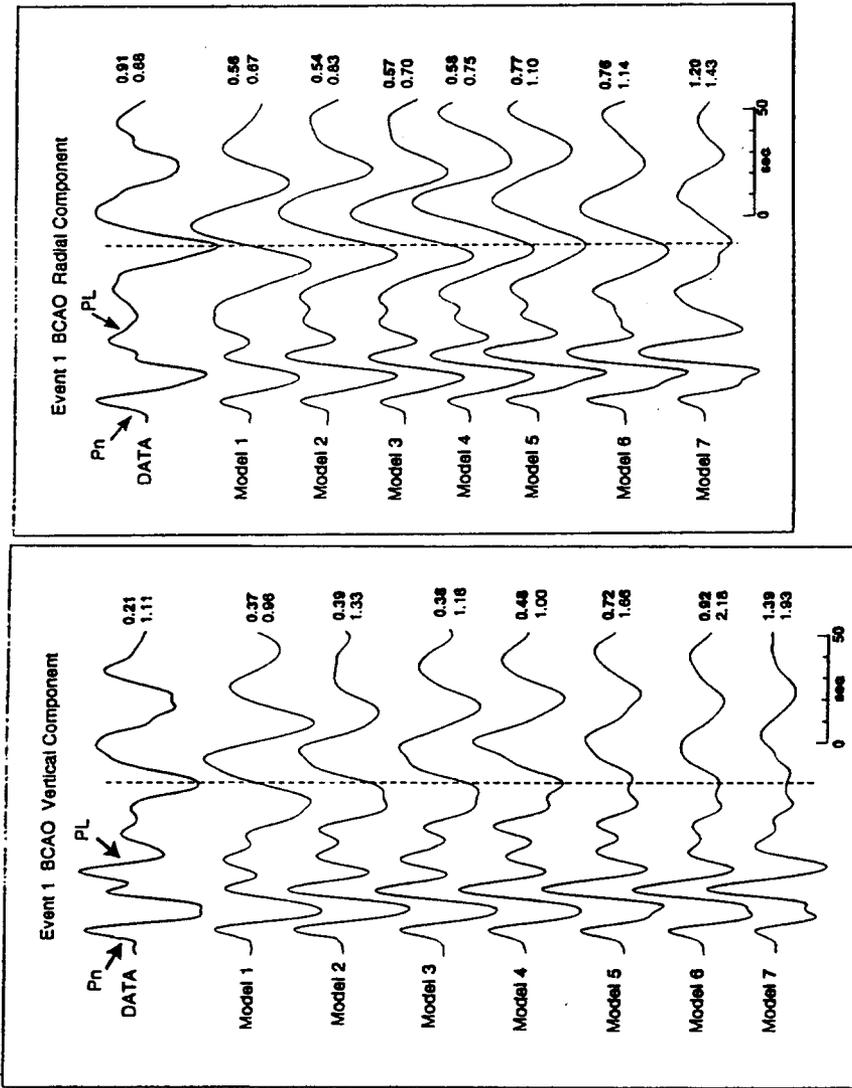| V_p (km/s)	V_s (km/s)	ρ (g/cm^3)	Q_p	Q_s	Thickness (km)
6.10	3.52	2.72	1000	440	15
6.25	3.61	2.77	1000	440	10
6.65	3.84	2.90	1000	440	15
8.05	4.64	3.35	500	220	half-space

Figure 2. Data (top bold trace) and synthetics for Event 1; (a) vertical component, (b) radial component. Traces are aligned on the first upswing (P_n) and have been low-passed filtered at 0.3 Hz. The top number to the right of each trace gives the maximum amplitude in microns and the bottom number is the P_n/PL amplitude ratio. A reference line (dashed) aligned on the first large downswing of the PL phase illustrates the arrival time of PL relative to P_n.
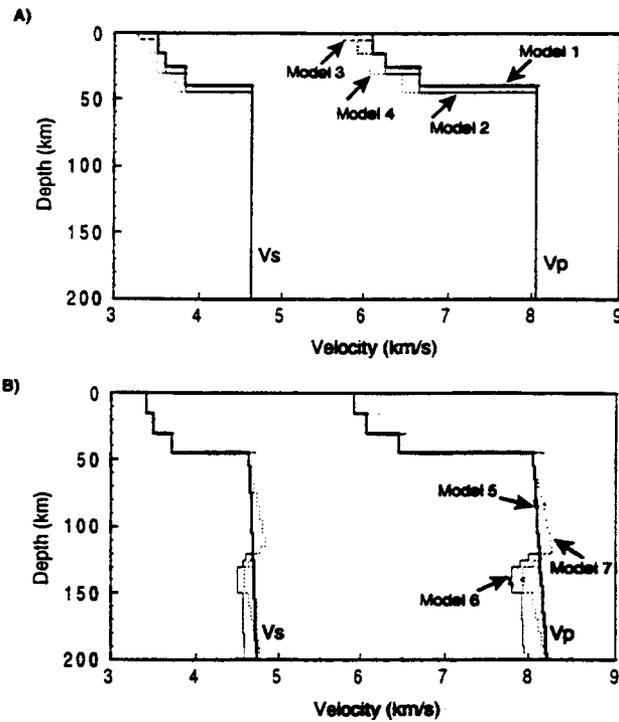

Figure 1. Map of the southern African subcontinent showing the Precambrian tectonic framework (after Hartnady et al., 1985), the northern boundary of the African superswell, and the location of seismic stations (solid triangles) and earthquakes (solid stars) used in this study. Archean cratons are shaded, the boundaries of the Proterozoic mobile belts are delineated with dashed lines, and the Congo Basin is shown with a stippled pattern.

Figure 3. Radially symmetric velocity models used to construct synthetics for Event 1; (a) crustal models, (b) upper mantle models.
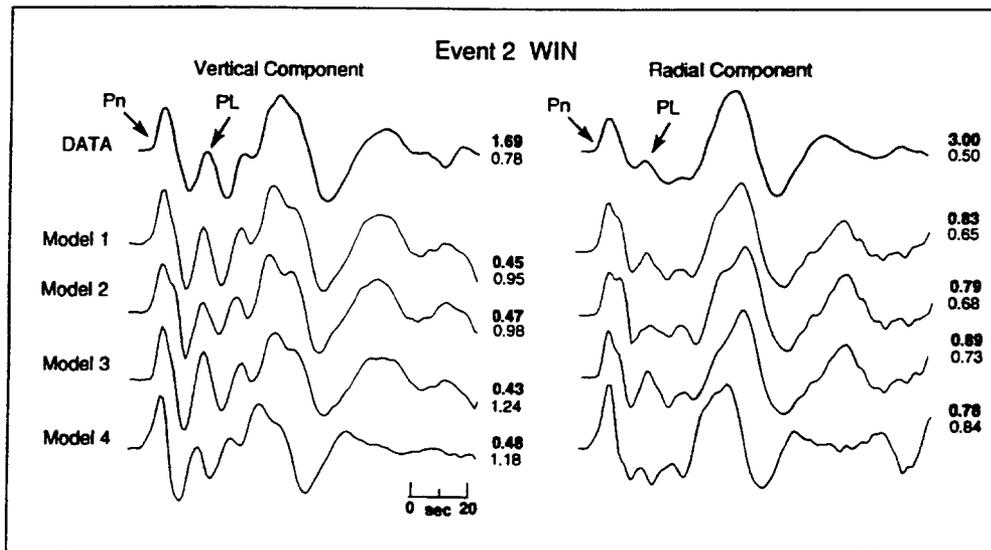

Figure 4. Data (top bold trace) and synthetics for Event 2. Traces are aligned on the first large upswing (P_n). Numbers to the right of each trace are the same as in Figure 2.

278

Event 3 WIN

Vertical Component

Pn   PL

DATA   **1.01**
        1.00

Model 1   **0.29**
          0.88

Model 2   **0.37**
          0.98

Model 3   **0.44**
          1.09

Model 4   **0.45**
          0.71

0   sec   20

Radial Component

Pn   PL

1.17
1.03

0.40
0.80

0.41
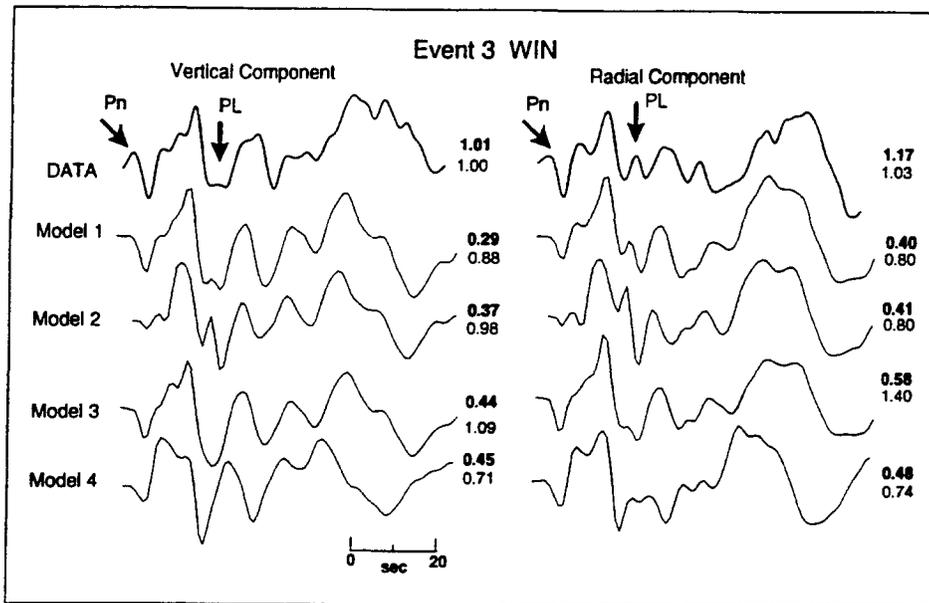0.80

0.58
1.40

0.48
0.74

Figure 5. Data (top bold trace) and synthetics for Event 3. Traces are aligned on the first large downswing (P_n). Numbers to the right of each trace are the same as in Figure 2.
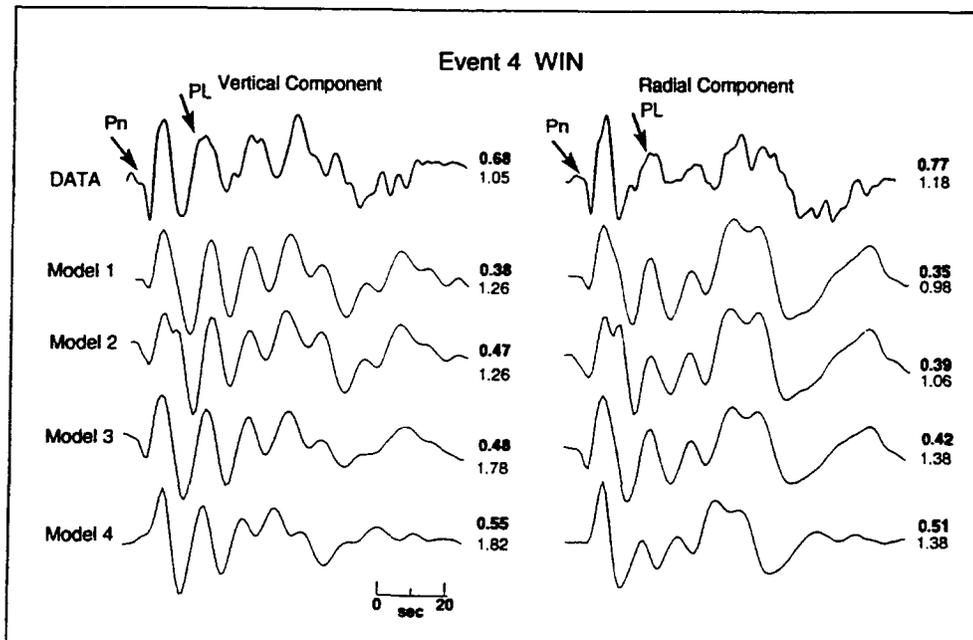
Event 4 WIN

PL   Vertical Component

Pn

DATA   **0.68**
        1.05

Model 1   **0.38**
          1.26

Model 2   **0.47**
          1.26

Model 3   **0.48**
          1.78

Model 4   **0.55**
          1.82

0   sec   20

Radial Component

Pn   PL

0.77
1.18

0.35
0.98

0.39
1.06

0.42
1.38

0.51
1.38

Figure 6. Data (top bold trace) and synthetics for Event 4. Traces are aligned on the first large downswing (P_n). Numbers to the right of each trace are the same as in Figure 2.
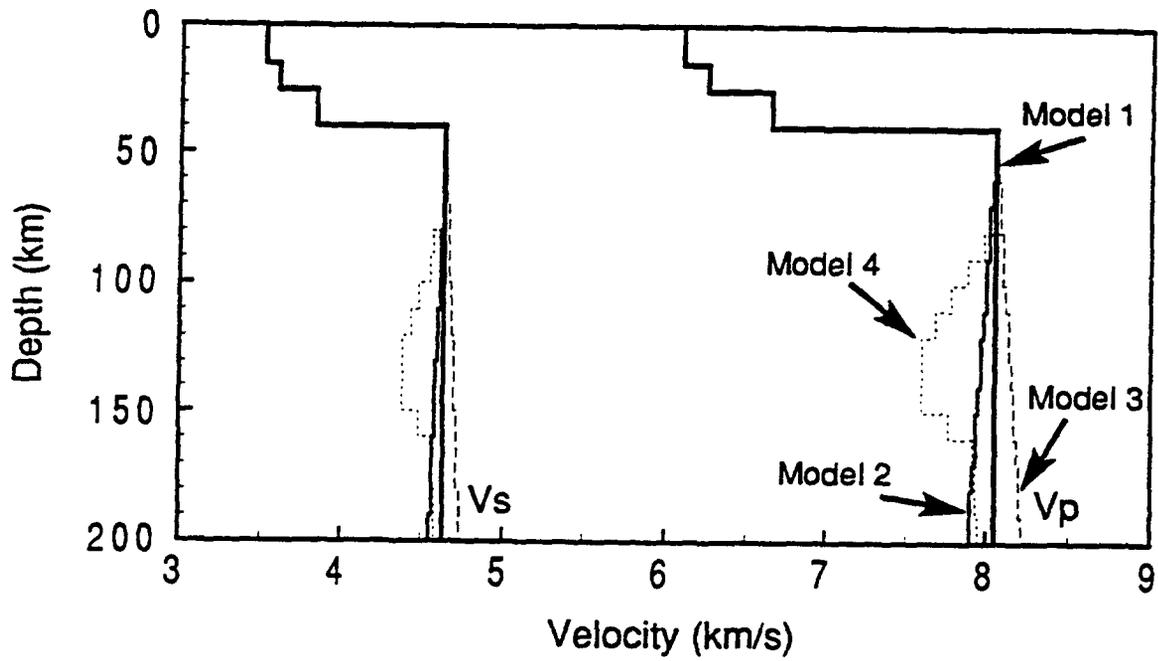
279

Figure 7. Velocity models used to construct the synthetics in Figures 4, 5, and 6.